11.2 Global Issues

11.2.1 Introduction

The ATLAS SCT aims to operate reliably according to performance specifications over a 10-year period of high luminosity LHC operation. The design LHC luminosity aims for an average peak value of 10^{34} $cm^{-2}s^{-1}$ over 10^7 secs per year, giving an annual integrated luminosity of 10^{41} cm^{-2}. Instantaneous rates may exceed this value. These luminosities are achieved using bunch-bunch crossings separated by 25 nsec (40 MHz) to result in a particle interaction rate ~10^9 Hz.

The Inner Detector must also be capable of precision tracking and secondary vertex detection at initial 'low' luminosities (~$10^{33}cm^{-2}s^{-1}$), for physics studies of the long-lived B-meson and B-hadron systems. Since the Technical Proposal [11-3], the necessity of b-quark tagging at high luminosity has also become evident, for SUSY studies and for possible B-decays of the Higgs (see for example Chapter 2.4.3). As a result, at least one semiconductor (pixel) layer should be as close as possible to the beam pipe (a nominal radius 4cm) in order to measure the impact parameter of b-quark decays precisely.

The overall Inner Detector layout is shown in Figure 1-i and Figure 1-1 of Chapter 1.2.2, together with the actual layout of the SCT. The SCT radial envelope is defined internally by the tolerance of silicon sensors and their electronics to charged and neutral radiation, and externally by the TRT, to an active radius r < 52 cm in the barrel region and r < 56 cm for the forward silicon disks. The SCT must meet stringent performance criteria of occupancy, two track resolution, momentum resolution and detector efficiency that are summarised below in Section 11.2.2, and discussed in detail in Chapter 2.

Silicon has been chosen as the detector medium because of its fast signal speed, and excellent spatial segmentation. The RD2 [11-4], RD20 [11-5] and SSC [11-6] programs, and subsequent R&D within ATLAS (see [11-3], for example), have demonstrated that silicon sensors can survive long-term high luminosity operation. Nevertheless, despite experience gained by the implementation of micro-vertex detectors at LEP and at the Tevatron Collider, substantial developments have been required:

- Acceptable fluence levels to maintain a satisfactory signal-to-noise ratio in silicon detectors have been determined, together with an understanding of consequent operating conditions (bias, cooling, etc).
- Developments of fast, low-noise and low-power on-detector electronic components have been made in radiation hard technologies.
- Fast signal processing has been developed to separate signals from successive bunch crossings. A fast recovery time minimises the loss of signals in subsequent bunches, and pipelining with simultaneous read-write functionality and subsequent fast data links minimises dead time.
- Substantial engineering studies have been made to enable dimensional stability of the full SCT and its component parts, following repeated temperature cycling over a range of >30°C. An interferometric alignment system will follow the effect of environmental changes in the tracker.
- The optimisation of the layout and readout allows the use of the SCT as part of the 2nd-level event trigger; the good calorimetric 1st-level trigger rejection and the 100 kHz bandwidth of the 1st-level trigger precludes the need to use it there.

The design presented in this report aims to satisfy all these requirements. Despite the high granularity of the silicon detectors, and the high density of services, the material in the SCT (and in all parts of the ID) must not significantly deteriorate the electromagnetic calorimeter resolution, nor the pattern recognition and electron identification capabilities of the ID.

In Section 11.2.3, the charged and neutral fluences are described. Also introduced in this Section are global concerns of access, services and material. In Section 11.2.2, the SCT layout, and specifications justifying the layout, are presented. Parameters of the layout are tabulated in that Section, and consequent design implications are described in Section 11.2.4.

11.2.2 Motivation and Description of the Layout

The layout of the Inner Detector and the SCT are shown in Figure 1-1. Using this layout, extensive performance studies have been made, using nominal performance parameters for the detectors. These studies are documented in Chapter 2, and are not discussed here. In this Section, we briefly recall key physics requirements determining the most important detector specifications and layout.

Requirements for the full ID translate in the case of the SCT as follows:

- The reconstruction of isolated leptons of $p_T > 5$ GeV with an efficiency of 95% in the range $|\eta| < 2.5$ and with a fake track rate of < 1%, imposes the need to reconstruct helices in 3D (especially since the TRT has no stereo capability). This imposes on the combined SCT and pixel system the need for at least six tracking layers able to provide space point information, and a detector efficiency over the lifetime of the experiment of > 95%, to ensure good tracking and trigger efficiency.
- The $(\delta p_T/p_T) < 0.3$ requirement at $p_T = 500$ GeV with a beam constraint imposes an r-ϕ measurement accuracy of ~ 20 µm at the SCT radius. The requirement to separate multiple vertices within a bunch crossing imposes an accuracy on the z-measurement of < 1mm in the SCT. That constraint is made more stringent by requirements of K^0 reconstruction and mass resolution where a z-measurement of ~ 0.5 mm is required in the SCT.
- The requirement of 2-track resolution <200 µm at R=30 cm, in order to keep track losses in b-jets to <5%, also imposes a constraint on the r-ϕ readout pitch.
- As already noted, to minimise material effects preceding the calorimeter, the SCT and pixel layers must have a minimum radiation length compatible with their robust construction, with the aim of reaching <0.2 X_0 preceding the TRT, over a significant η range.

To satisfy these criteria, the SCT design assumes the geometrical configuration of Figure 1-i and Figure 1-1, with detailed parameters as given in Table 11-1 and Table 11-2. The layout consists of 4 'central' barrel layers in the radial range 30 < R < 52 cm, and 9 disks in each of the forward and backward directions in the radial range 26 < R < 56 cm.

In the barrel region, each layer consists of silicon strip modules of 4 single-sided silicon detectors with active area 61.6 x 62.0 mm^2, and geometric area 63.6 x 64.0 mm^2. Within the module, two detectors are daisy-chained for each side of a module. On one side 768 strips of 80 µm pitch and active length 123.2 mm are aligned precisely along the beam direction. The back-side detector pair is identical, but rotated by 40 mrad, to provide a z-measurement capability. The use of small-angle stereo rather than orthogonal strips is motivated by the need to reduce the number of ghost hits near a real track in high-multiplicity events. A second motivation is to retain an r-ϕ measurement capability in the case of detector inefficiencies. In order to minimise the signal

Table 11-1 Barrel Silicon Strip Characteristics.

Radius (mm)	1/2 length (mm)	Tilt angle (degrees)	Pitch (μm)	# modules	# channels	Total area (m^2)	Orientation
300.0	746.7	10.0	80.0	12 x 32	589824	2 x 3.13	Φ,u (40 mr)
373.0	746.7	10.0	80.0	12 x 40	737280	2 x 3.91	Φ,v
447.0	746.7	10.0	80.0	12 x 48	884736	2 x 4.70	Φ,u
520.0	746.7	10.0	80.0	12 x 56	1032192	2 x 5.48	Φ,v

Total modules: 2112

Total substrate area: 2 x 17.2 = 34.4 m^2

Estimated Power (detector+ electronics+ services): ~13 kW

Total channels 3,244,032

Modules are staggered in radius by ±1 mm to give overlap in z, and an overlap of 1% in ϕ makes the detector hermetic for p_T > 1 GeV/c. A dead space does remain between daisy-chained detectors.

Table 11-2 Forward Silicon Strip Characteristics

#	z (mm)	Radius (inner/outer) (mm)	Modules (I/M/O)	Channels	Total Area (m^2) (external)	Orientation
1	835.0	259-560	40/40/52	4*101376	4*0.8580	Φ,u (40 mrad)
2	925.0	336-560	-/40/52	4*70656	4*0.7109	Φ,v (40 mrad)
3	1072.0	259-560	40/40/52	4*101376	4*0.8580	Φ,u
4	1260.0	259-560	40/40/52	4*101376	4*0.8580	Φ,v
5	1460.0	259-560	40/40/52	4*101376	4*0.8580	Φ,u
6	1695.0	259-560	40/40/52	4*101376	4*0.8580	Φ,v
7	2135.0	336-560	-/40/52	4*70656	4*0.7109	Φ,u
8	2528.0	401-560	-/40/52	4*70656	4*0.55715	Φ,v
9	2788.0	440-560	-/-/52	4*39936	4*0.40405	Φ,u

Total Modules: 1976

Total substrate area 26.692 m^2 (including edges)

Estimated power (detectors + electronics + services): ~12 kW

Total channels: 3035136

A z-stagger of 0.5cm allows overlaps.

Pitch in μm (min/max):

Inner	**54.53/69.43**
Middle	**70.48/94.74**
Outer	**70.92/90.34**

spread during operation in a 2 Tesla solenoidal field, the modules are mounted at an angle of 10° to the tangent. Modules are overlapped in a tile arrangement to minimise dead areas in the barrel region. The silicon detector signals will be read out by binary front-end electronics, for reasons that are described in detail in Section 11.4. This choice dictated the readout of individual strips (rather than charge division), and therefore the 80 μm pitch (giving a point resolution in ϕ of < 23 μm, and a space point resolution $<15 \oplus 12\,\mu$m including alignment). Within the barrel region, all detectors have the same pitch, and all modules are identical.

In the forward direction, the geometrical layout no longer allows the use of identical detector designs; nevertheless, the module construction is similar. Modules of daisy chained single-sided detector pairs with strip length ~12 cm and mean pitch ~80 µm, are arranged back-to-back with a 40 mrad stereo orientation. As described in Section 11.3.2, 5 wedge-shaped detector designs are necessary.

Because of radiation damage to silicon detectors from the charged and neutral radiation, the detectors of both the barrel and forward regions will be operated at -7°C in a dry nitrogen environment. As a result, the structure is designed to remain stable following repeated thermal cycling between -15°C and 25°C.

11.2.3 Operating Environment

11.2.3.1 Event rates

As already noted, the dominant source of radiation at small radius comes from direct pp interactions. At a luminosity of 10^{34} cm^{-2}s^{-1}, typically 23 interactions occur per bunch crossing. The particles are produced approximately uniformly in rapidity, and with low p_T. Given the 2 Tesla solenoidal field of ATLAS, these low p_T particles ('loopers') traverse multiple SCT layers. Other charged radiation will result from subsequent material effects (photon conversions, nuclear interactions). Beam losses and beam-gas interactions contribute an order of magnitude less radiation than direct interactions at high luminosity. The charged particles are predominantly pions. Because of interactions in the calorimeter, albedo neutrons are also a significant source of radiation, being dominant at larger radii in the SCT.

Figure 11-1 shows the distribution of interactions per bunch crossing at a luminosity of 10^{34} cm^{-2}s^{-1}. Figure 11-2 shows the distribution in η of the produced particles, obtained using both the PYTHIA [11-7] and DTUJET [11-8] event generators. Using the detector parameters listed in Section 11.2.2, the GEANT3 [11-9] program and PYTHIA event generator have been used to evaluate the mean detector occupancies from charged particles. Results are listed in Table 11-3 for each barrel of the SCT and are below the average ~1% occupancy limit imposed by the SCT readout speed.

11.2.3.2 Radiation level

The procedure used to evaluate the fluence is to assume 3 years of low-luminosity operation (10^{33} cm^{-2}s^{-1} for 10^7 s/yr) followed by 7 years of high-luminosity operation (10^{34} cm^{-2}s^{-1} for 10^7 s/yr). A proton-proton inelastic (non single diffractive) cross-section of $\sigma_{pp} = 70$ mbarn is assumed. The DTUJET code has been used to generate minimum bias particles, and the FLUKA transport code [11-10] has been used to transport the produced particles, and treat their subsequent decays or interactions. An uncertainty of ± 50 % is nominally assigned to these fluences due to the combined uncertainties of the inelastic cross-section and the event multiplicity. Also included in this estimate are radiation damage corrections described below. It is noted that the generator discrepancy is within this uncertainty, with DTUJET on the low side.

Within FLUKA, a detector model has been constructed by Ferrari, which reproduces the location and quantity of material in the Inner Detector and Calorimeter regions [11-11]. In particular, beam-pipe supports and flanges, the detector supports and services, the forward neutron moderator and the integrated forward calorimeter are modelled. Since the bulk radiation damage to

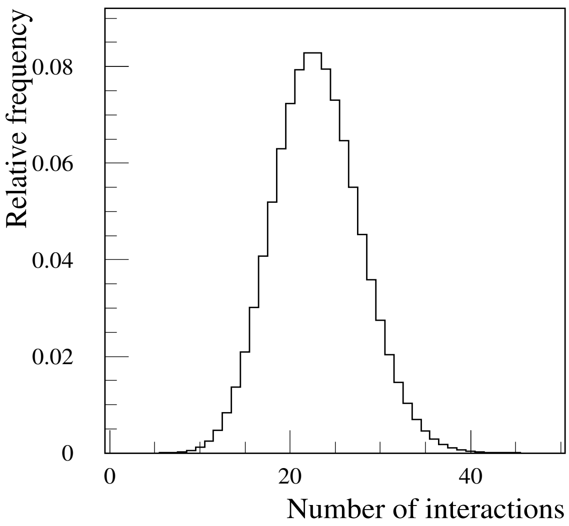

Figure 11-1 Distribution of the number of interactions per bunch crossing at a luminosity of $10^{34}cm^{-2}s^{-1}$.

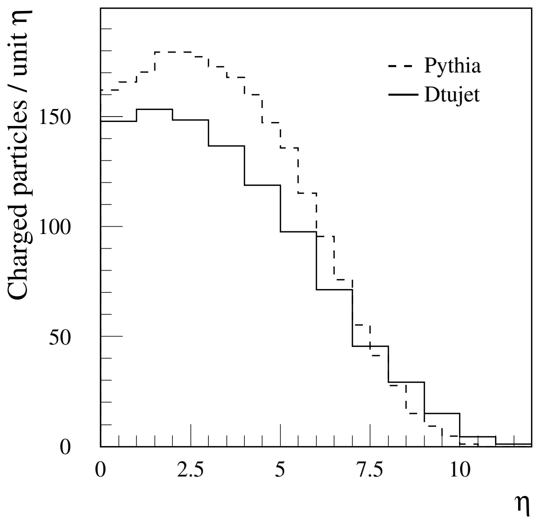

Figure 11-2 Distribution in η of charged particles produced per bunch crossing at a luminosity of $10^{34}cm^{-2}s^{-1}$. Results are shown for both the DTUJET and PYTHIA minimum bias event generators.

silicon dominantly results from the non-ionising inelastic cross-section (NIEL), it is convenient to normalise the fluences to a fixed energy and particle type, historically 1 MeV neutrons. The most recent NIEL neutron damage normalisation functions [11-12] have been used in this evaluation, together with the charged particle normalisation functions of Huhtinen et al. [11-13], [11-14]. The total neutral and charged particle fluence, normalised to the 1 MeV equivalent neutron fluence, is shown in Figure 1-iii. The instantaneous fluence of charged hadrons is shown in Figure 1-iv. The results are averaged over ϕ. The fluences appropriate to each SCT detector element are listed in Table 11-3 and Table 11-4.

Although the neutron fluences have been evaluated to low energy, only neutrons with energy >100 keV are used in the damage calculations, since the damage cross-section drops significantly at lower energies. The energy spectra of charged pions, neutrons and photons are shown in Figure 11-3. From these fluence values, with a parametrisation of the detector performance as a function of the fluence, the required depletion (and operational) voltage of the silicon detectors can be estimated. Results are described in Section 11.3.1.

Detailed comparisons with previous estimates [11-3] indicate a significant reduction of the neutron fluence. This results from an improved contiguous forward moderator design, a more favourable calorimeter plug geometry and a new increased estimate for the hydrogen content of the Inner Detector. Furthermore, neutron and proton damage cross-sections have recently been revised downwards [11-12], [11-13]. The sensitivity of the neutron fluence and therefore silicon damage makes it a critical parameter in detailed design optimisations and subsequent construction controls.

Table 11-3 Estimated barrel occupancy, and annual fluence after normalisation to the damage of 1 MeV neutrons, at a luminosity L=10^{34} cm^{-2}s^{-1}. The occupancy is estimated using the PYTHIA generator, and DTUJET is used to evaluate the fluence. The fluence has an estimated uncertainty of ±50 %.The typical point-to-point statistical uncertainty of ±(5 – 10) % is not listed.

	Occupancy (%)	Fluence (neutral) x 10^{12} n_{eq}/cm^2		Total Hadron Fluence (10^{12} n_{eq}/cm^2)		Total Hadron Fluence after 10 yrs (10^{14} n_{eq}/cm^2)	
	z=0 cm	z=0 cm	z=75 cm	z=0 cm	z=75 cm	z=75cm	Design value
Barrel 1	0.64	8.9	9.2	17.5	17.8	1.30	1.95
Barrel 2	0.50	7.4	8.1	13.4	14.1	1.03	
Barrel 3	0.40	7.3	7.1	11.7	11.6	0.85	
Barrel 4	0.33	6.4	7.0	9.8	10.5	0.77	

Table 11-4 Estimated SCT annual fluence after normalising to the damage of 1 MeV neutrons, at a luminosity L=10^{34} cm^{-2}s^{-1}. DTUJET is used to evaluate the fluence. The fluence has an estimated uncertainty of ±50 %. The typical point-to-point statistical uncertainty of ±(5 – 10) % is not listed.

		Max Neutral Fluence (10^{12} n_{eq}/cm^2)	Total Hadron Fluence (10^{12} n_{eq}/cm^2)	Total Hadron Fluence after 10 yrs (10^{14} n_{eq}/cm^2)	Design value after 10 yrs (10^{14} n_{eq}/cm^2)
Disk 1	Module 1	9.2	19.6	1.43	2.14
	Module 2	9.8	16.9	1.23	1.94
	Module 3	8.4	12.5	0.91	1.86
Disk 2	Module 2	7.9	15.2	1.11	
	Module 3	7.4	11.6	0.85	
Disk 3	Module 1	8.8	18.6	1.36	
	Module 2	8.0	15.0	1.10	
	Module 3	7.0	11.3	0.82	
Disk 4	Module 1	7.8	17.7	1.29	
	Module 2	8.3	15.6	1.14	
	Module 3	6.9	11.2	0.82	
Disk 5	Module 1	8.6	18.4	1.34	
	Module 2	8.7	15.7	1.15	
	Module 3	7.8	12.1	0.88	
Disk 6	Module 1	9.0	19.0	1.39	
	Module 2	8.1	15.4	1.12	
	Module 3	7.6	12.0	0.88	
Disk 7	Module 2	9.1	16.5	1.20	
	Module 3	8.7	13.2	0.96	
Disk 8	Module 2	10.7	16.8	1.23	
	Module 3	10.6	15.2	1.11	
Disk 9	Module 3	12.2	17.0	1.24	

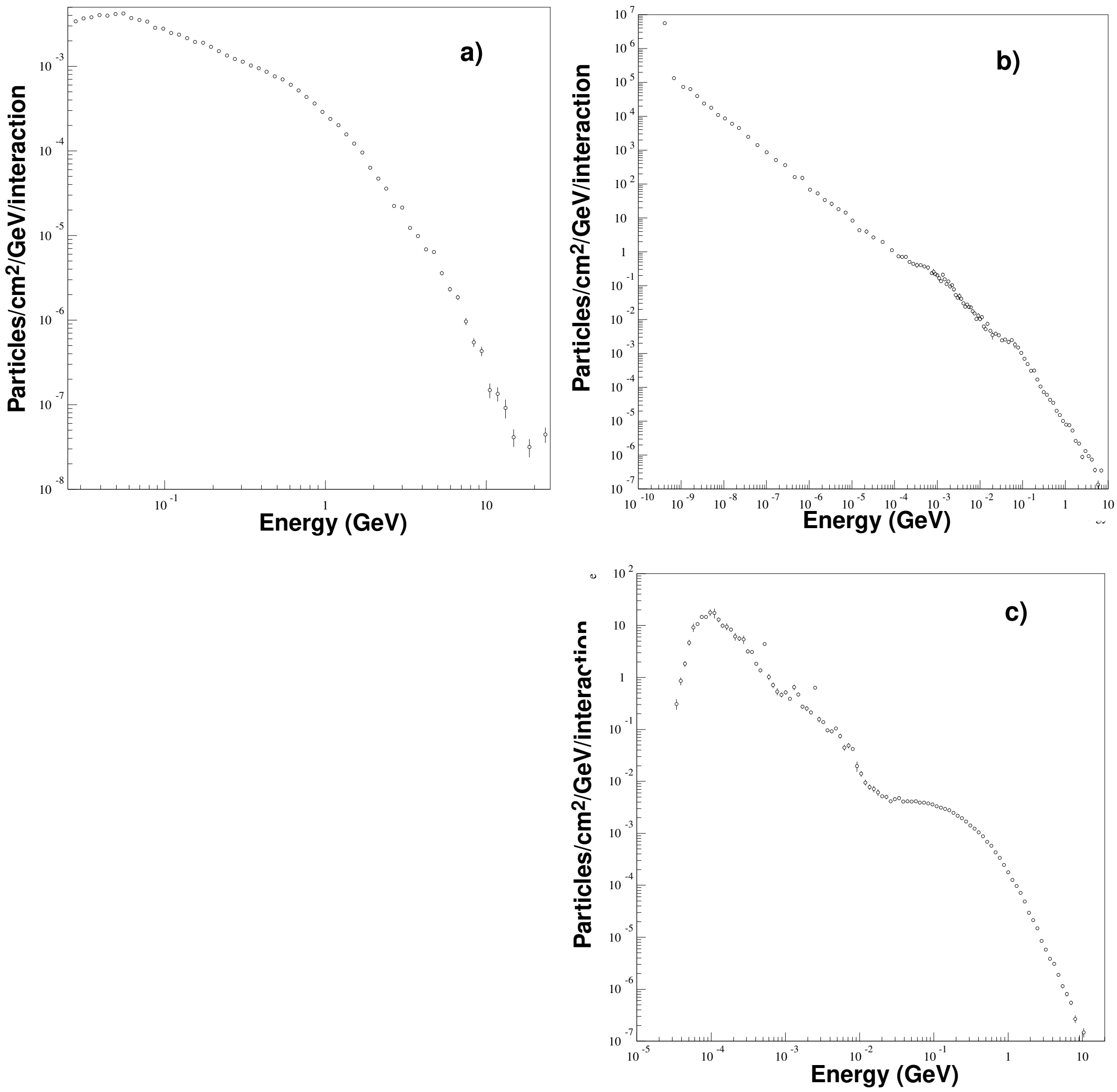

Figure 11-3 Energy spectrum at the 1st barrel for (a) charged π, (b) neutrons, and (c) photons. The energy scale is in GeV.

The radiation doses also impact the detector design in other areas:

- The design and characterisation of front-end and data transmission ICs in radiation hard technologies (the Bi-CMOS DMILL process in France [11-15], or alternatively the Honeywell CMOS and Maxim bi-polar processes [11-16], [11-17] in the US), is discussed in Chapter 13.
- The data transmission electronics; light diodes, pin diodes and optical fibres must be radiation hard, as discussed in Section 11.4.
- The certification of all structural materials, including adhesives, thermal-conduction paths, insulation, etc, is required. Some prototype studies are noted in Section 11.12.5.

11.2.3.3 Access, services and maintenance

To provide power and signal transmission for the SCT detector, which has nearly 6 x 10^6 channels, is a formidable task. For this reason, as is described in Section 11.4, special developments have been made to:

- maintain stringent low-power specifications for all on-detector electronics, and
- customise cables and services to the SCT, to minimise space and material, and to minimise power losses.

Despite this, power losses from the electronics and power transfer from the silicon detector leakage current is expected to reach ~30 kW within the thermal enclosure, with an additional power load from the pixel detectors. Due to radiation damage, the silicon detectors must furthermore be maintained at an operating temperature of -7°C. The surrounding TRT will be operated at room temperature. As described in Section 11.7 and Section 11.12, cooling channels will contact each detector module. The consequent pipework must be removable for access, and have a small radiation and absorption length.

It is inevitable that access to the Inner Detector will be limited, and since radiation damage is severe, redundancy must be included in the system design. Nevertheless, access will be required at regular intervals. A realistic access scenario has significant consequences on the size, number and robustness of all the service connections, on the structure of the thermal enclosures, and on the warm up time needed for detector maintenance.

11.2.3.4 Material

As noted many times in this Report, the Inner Detector material budget, both in terms of radiation length and absorption length, is larger than most existing tracking detectors. Figure 1-9 of Figure 1.2.4 indicates a total reaching 0.4 X_0 at the outer SCT envelope. As shown in Section 11.9, strenuous efforts have been made to minimise the material in both the modules and services of the SCT.

11.2.4 Design Choices for the SCT

The technical solutions for the SCT consist of a choice of silicon detector design and technology, a choice of front end, readout, and monitoring electronics, a detector module design, a data transmission and cabling technology, a mounting scheme, and a cooling system.

Detectors

The effects of heavy particle irradiation on silicon detectors are documented in Section 11.3. These include an increase in leakage current, a change in effective doping, and a decrease in charge collection efficiency. The change in effective doping implies a change in the voltage necessary to deplete the detector and for detectors which are built on *n*-type bulk, the doping change will result in an effective type inversion. Projections for the SCT after 10 years of operation indicate depletion voltages of up to ~ 450 V and type inversion for all sensors. Significant uncertainties exist which may imply even higher voltages.

By constructing n-in-n detectors (n+ strips on an n-type substrate) it has been demonstrated (Section 11.3) that efficient partially depleted operation is possible after type inversion, with fast signal collection and limited charge diffusion. Because of the consequent safety margin, single sided n-in-n sensors have been chosen. The detectors will be AC-coupled, and will be negative-biased from the backside to maintain only a small voltage across the capacitor oxide.

Electronics

The front end electronics is based upon a one-bit digital (binary) readout architecture. This choice is supported by test-beam and bench prototype studies, and is the most cost-effective implementation meeting the performance requirements. Any strip which collects charge above an externally adjustable threshold fires a per strip discriminator. The binary output is stored in a pipeline until an ATLAS trigger initiates readout for that beam crossing. A consequence for this architecture is significant data reduction in the front end chips, meaning that the discriminator performance, thresholds, noise, and pickup must be well controlled.

The hybrid design uses a thick film technology on a Beryllium Oxide (BeO) substrate. The substrate choice is motivated by the high thermal conductivity and long radiation length of this material.

An optical communication scheme is chosen, because of its low mass and lack of electrical pick-up. It is required, however, to be radiation resistant. Each pair of hybrids is connected to a pair of light-diode (LED) drivers which share the output data. In case of failure, one driver can be used for the pair. The clock and control data are received optically by a PIN diode near the hybrid. The SCT cable design for low voltages and detector bias uses a thin aluminium on kapton technology. This is chosen to minimise mass while maintaining an acceptable voltage drop.

General ATLAS design considerations have resulted in a deadtime-less readout, and this has forced simultaneous read-write operations on the front-end pipeline. The readout speed is defined by the 100 kHz level-1 trigger rate, since the tracking data are used for level-2 trigger decisions.

Power supplies for the SCT are segmented to provide self contained low and high voltage channel separately to each module. The SCT design specifies a “groundless” system which serves to maintain maximum isolation between each module. This minimises pick-up and potential ground loops. High impedance DC connections are included to prevent excessive baseline drift between components.

Modules

A module is the basic readout unit of the SCT. The module layout is described in Section 11.2.2 and in Section 11.5; two pairs of daisy-chained detectors are glued back-to-back with one pair rotated by 40 mrad. The readout of 12-cm strips was motivated by cost, while maintaining adequate signal-to-noise (S/N) performance. To minimise the effect of strip resistance and fan-out capacitance on the S/N, a ‘centre tapped r-ϕ’ design, where the front end IC’s are bonded at the middle of the module, is chosen for the barrel. Mechanical assembly is more complex for the forward modules, and an ‘end tapped’ design is chosen, at the expense of a modest increase in noise.

Cooling considerations significantly constrain the module design. In order to avoid the thermal runaway of damaged silicon detectors, a thermal base board is required to increase the effective in-plane thermal conductivity. There must also be good thermal contact to the cooling pipes.

Calibration and monitoring

In order to monitor the front-end electronics, in order to avoid the thermal run-away of damaged detectors, the SCT requires a calibration and monitoring system. The calibration system will be embedded in the DAQ system, and will allow the measurement and monitoring of critical parameters such as the front end-noise, gain and threshold. Variations can be a sign of radiation damage or electrical problems. A separate slow DAQ system will monitor operating conditions such as supply voltages and currents, temperatures, radiation levels, and cooling functions.

For safety reasons, critical safety functions will be controlled by hard wired circuits.

Cooling

The silicon detectors, front-end electronic hybrids, and cables must be cooled to control leakage current, radiation induced doping changes, and to remove heat generated by front end chips and DC voltage drops. Binary ice is chosen as the primary coolant, since it cools by the ice-water phase transition and therefore offers near isothermal performance.

To reduce temperature variations, and detector breakdown, the SCT will be surrounded by a thermal enclosure, and maintained in a dry, cold nitrogen atmosphere.

Support structure

The SCT support structure must maintain dimensional stability following temperature variations of up to 30°C. To ensure this, the SCT barrel and disk supports will be constructed from 0-CTE material. This will be achieved using a carbon fibre skin and honeycomb core composite, tuned to have a coefficient of thermal expansion near zero. The barrels are interlinked by flanges of zero CTE material. In the case of the barrel, groups of modules will be mounted on the outer barrel surface using non-structural local support members, while for the disks, modules will be directly mounted on the support structure.

Since the low mass cooling pipes are of aluminium, these pipes must be mounted flexibly on the supports, while the modules will be mounted using precision pins.

The forward disks are supported in groups, within an external space frame structure.

11.2.5 References

11-3 ATLAS Technical Proposal, CERN/LHCC/94-43, December 1994.

11-4 RD2 Collaboration, R&D Proposal CERN/DRDC/90-27 (August, 1990),
RD2 Collaboration, Final Report of the RD2 Project, CERN/LHCC/96-5 (January 1996).

11-5 RD20 Collaboration, R&D Proposal CERN/DRDC/91-20 (1991),
RD20 Collaboration, RD20 Status Report, CERN/DRDC/94-39 (1994).

11-6 SDC Collaboration, Technical Design Report, SDC-92-2-1 (April 1992).

11-7 PYTHIA 5.7, T. Sjostrand, CERN preprint CERN-TH7111/93 and CERN-TH7112/93

11-8 F.W. Bopp et al., Phys. Rev. D49 (1994) 3236.
P. Aurenche et al., Phys. Rev. D45 (1992) 92.

11-9 GEANT3 Detector Description and Simulation Tool, CERN Program Library long writeup, W5013, 1994.

11-10 A. Fasso et al., Proc. 4th. Intl. Conf. on Calorimetry and their Applications, World Scientific, Singapore (1994) 493.

11-11 A. Ferrari, private communication. See also [11-3].

11-12 P.J. Griffin, private communication.
This evaluation uses the ENDF/B-VI revision 4 cross-sections, and the methodology of P.J. Griffin et al., SNA RML Recommended Dosimetry Cross Sections, Sandia National Laboratories Report SAND92-0094.
See also:
A. Vasilescu, " The NIEL scaling hypothesis applied to neutron spectra of irradiation facilities and in the ATLAS and CMS SCT", ROSE Collaboration Technical Note ROSE/TN/97-2 (Febuary 1997).

11-13 M. Huhtinen et al., Nucl. Instr. Methods A335 (1993), 580.

11-14 G. Lindstroem, private communication.

11-15 DMILL technology, M. Dentan et al., First Workshop for LHC Experiments, CERN/LHCC/95-56 (October 1995) 41.

11-16 Bulk Ricmos-IV Process, Honeywell Corporation.

11-17 CB2 Process, Maxim Corporation.